ISSN: 1999-6691, e-ISSN: 2782-3709 DOI: 10.7242/1999-6691/2026.19.1.5

Research article

Implementation of a C^1-continuous finite element method within strain gradient elasticity for crack problems

K.A. Shelkov[1], ***Y.O. Solyaev***[1,2]

[1] *Moscow Aviation Institute (National Research University), Moscow, Russian Federation*
[2] *Institute of Applied Mechanics of the Russian Academy of Sciences, Moscow, Russian Federation*

Strain gradient elasticity (SGE) offers the possibility of regularizing a wide class of problems in classical solid mechanics, including those involving cracks, sharp corners, concentrated loads, dislocations, etc. Within the framework of SGE, it is assumed that the strain energy density depends not only on the strains themselves but also on their spatial derivatives, which imposes additional smoothness requirements on the strain and stress fields realized in SGE solutions. This work presents an implementation of a C^1-continuous finite element method, based on a simplified strain gradient elasticity theory, in the Abaqus/CAE software suite. Standard and enriched three-node elements are presented; 5th-order polynomials are used as shape functions. The implementation was carried out using a user subroutine UEL and a custom user interface. Based on calculations performed for mode I, mode II, and mixed-mode crack opening problems, the mesh convergence of the obtained solutions is investigated, and estimates of the stress distribution near the crack tip are provided. The computational efficiency of the enriched elements compared to the standard ones is also demonstrated, due to their faster convergence rate. The use of enriched elements allows for obtaining the amplitude coefficients of the asymptotic SGE solutions, which, in turn, enable the calculation of the J-integral and the application of energy criteria from linear fracture mechanics while accounting for the size effect.

Keywords: Strain gradient elasticity, crack problems, asymptotic solutions, fracture mechanics, numerical modeling, UEL subroutine, enriched elements

Received: 22.12.2025 / *Published online*: 01.06.2026

1. Introduction

When developing new types of engineering structures, ensuring the strength of the future product is a crucial stage. One of the main causes of loss of load-bearing capacity in a structure is the initiation and growth of defects and cracks in regions of stress concentration. Stress concentrators, such as crack tips, sharp corners, regions with concentrated loads, or regions with nonuniform (nonsmooth) boundary conditions, are characterized by nonphysical singularities in the stress and strain fields revealed by classical analysis methods (within the framework of linear elasticity) [1–3]. Their description requires the use of fracture mechanics, and, in a more general case, nonlinear fracture mechanics or other approaches whose application requires additional material constants and complicates strength analysis. When numerical methods are used, for example the finite element method (FEM), neither regularity nor mesh convergence can be ensured in the stress concentration zone [2, 4–6]. To address this problem, a wide range of methods based on classical approaches and theories has now been developed: linear elastic fracture mechanics (the virtual crack closure technique — VCCT, and the extended finite element method — XFEM), cohesive models, and progressive damage and failure models (see [7–12]). However, these methods have several drawbacks (initial cracks must be introduced, model geometry must be smoothed, and additional model parameters must be determined) and require their combined use when performing a complete analysis of damage initiation and evolution. All this substantially complicates the computational procedure. These methods also provide information on the stress and strain state in the stress-concentrator zone only through indirect parameters (the stress intensity factor — SIF, and the J-integral), while not eliminating the singularity problem. The difficulties inherent in classical theories arise from the failure to account for the large strain gradients that occur and from the absence, in the constitutive equations, of length scale parameters specifying the characteristic dimensions of the objects under study [13, 14].

©Authors 2026 Translation of the original article in Russian This is an open access article under the CC BY 4.0 license

Strain gradient elasticity (SGE), being a rigorous generalization of classical elasticity theory, makes it possible to regularize a wide class of problems and overcome the drawbacks of classical theories by assuming that the strain energy depends not only on the strains themselves but also on their spatial derivatives [1, 3, 7]. This makes it possible to solve macromechanical problems that have singular and nonsmooth solutions within classical theories (problems involving cracks, sharp corners, concentrated loads, dislocations, and others) by transforming them into problems with regular solutions.

The idea of using additional higher-order derivatives in constitutive relations was first proposed by Cauchy in the 1850s to correctly describe discrete lattice models [14]. Interest in SGE then revived in the 1960s. Since that time, its approaches and methods have been intensively developed by both the Soviet [15–17] and Western [1, 18–20] scientific schools.

In recent decades, SGE has continued to develop actively. Thus, [13] presents a simplified gradient theory and formulates SGE for finite and infinitesimal strains. Its main difference from previous approaches lies in the number of additional material constants, which was made possible by retaining only those higher-order terms that describe specific physical phenomena [1]. With the development of computing technology, numerous studies have appeared that apply numerical methods based on SGE to the analysis of complex structures [1, 21, 22]. In [23–27], the possibility of using SGE solutions to determine ultimate stresses in specimens made of orthotropic materials (glass- and carbon-fiber-reinforced plastics) and brittle isotropic materials with cracks of different lengths under various loading conditions was demonstrated. Since the solution obtained using SGE is nonsingular, the SIF and, consequently, the ultimate stress can be expressed through the parameter s introduced into the SGE solution, which represents a structural (scale) parameter. The parameter s is identified from physical tests. It is then assumed that this parameter is independent of crack size, and this assumption makes it possible to calculate ultimate stresses for specimens with other crack sizes. The ultimate stresses calculated in this way agree with experimental data within an error of 5% [23]. In [28], an SGE solution is demonstrated for a circular membrane loaded by a concentrated force. A regular solution is obtained that eliminates the singularity of the classical solution by accounting for a structural (scale) parameter determined experimentally. The ability to regularize solutions for a wedge-shaped plate subjected to a concentrated load is discussed in [29]. In [30], the refinement of the classical solution using the mathematical apparatus of SGE is shown for the problem of bending of a one-dimensional beam. Smooth regular solutions are constructed in the regions of the concentrated load and supports. It is established that SGE solutions make it possible to obtain refined, bounded stress and strain fields in stress concentration zones.

In [31–33], the ability of SGE to provide nonsingular solutions at crack tips and to perform strength analysis based on stress levels without using linear elastic fracture mechanics methods is also demonstrated, making it possible to develop a unified approach to studying static and fatigue cracks of arbitrary size. The obtained results were validated against experimental data for static loading of ceramics [31], fatigue loading of metals [32], and fatigue loading of concrete [33]; in this case, the characteristic grain size served as the length scale parameter for metals, while the mean size of the aggregate (crushed stone) was used for concrete. Estimates of the length scale parameter values that can be used when selecting model parameters in applied calculations are presented in [23, 34, 35].

The relevance of developing FEM approaches based on SGE by approximating solutions near concentrators with extended sets of approximating functions that satisfy the equilibrium (motion) equations of SGE lies in the possibility of creating hybrid finite-element (FE) solvers free from mesh divergence and nonphysical singularities. In essence, this is an alternative to existing methods of singular finite elements and the extended finite element method (XFEM), the virtual crack closure technique (VCCT), and FEM with cohesive elements [3]. The proposed approach eliminates the limitations of existing methods, generalizes classical hybrid FEM formulations, and reliably describes the features of changes in stress concentration and nominal strength of a material containing defects of different scales, down to cracks of microscopic dimensions.

Thus, the aim of this work is to demonstrate the solution of an SGE problem in Abaqus/CAE using two types of finite elements: type 1 — three-node elements with C^1-continuous approximation of the solution at the nodes, proposed in [21] (hereinafter referred to as standard elements); type 2 — also three-node elements, but referred to as enriched elements [22]. Solutions of crack problems using elements of the first type exhibit sufficiently stable behavior; however, their implementation requires a very high FE mesh density near the crack tip [22]. In the later proposed FEM modification based on enriched elements, the latter are placed near the crack tip and have additional shape functions corresponding to asymptotic solutions of SGE crack problems [22]. Similar classical elements are also called singular elements, and their

additional shape functions are asymptotic fracture mechanics solutions for cracks [36] or, in a more general formulation, Williams asymptotic series [37, 38]. In this case, the amplitude coefficients of the asymptotic solution (in particular, the SIF) become additional nodal variables of the model.

At present, in the standard FEM implementation for crack problems, so-called quarter-point elements are used — elements with points shifted from the midpoint of a side toward the vertices by one quarter of the side length. Such elements are simpler in numerical implementation and provide the required form of the shape functions near the crack tip [39, 40]. In SGE problems, introducing analogous elements with shifted nodes is difficult because the asymptotic behavior of the solution is fundamentally different from that of the singular classical solution [41, 42]. In order to use enriched elements, a scheme was proposed in SGE that makes it possible to preserve C^1-continuity of the solution between enriched and standard three-node elements. This paper presents a description of an implementation based on enriched elements that allows the Abaqus pre-/postprocessor and solver to be used, substantially improves the efficiency of the numerical scheme being implemented, and ensures its suitability for large-scale FE models as well as its potential application in both engineering analysis and fundamental research.

2. Problem statement

2.1. Simplified strain gradient elasticity

According to the classical provisions of SGE, the strain-energy density depends not only on the strains themselves but also on their first derivatives [18]:

$$w(\varepsilon_{ij},\varepsilon_{ij,k}) = \mathrm{C}_{ijkl}\varepsilon_{ij}\varepsilon_{kl}/2 + \mathrm{A}_{ijklmn}\varepsilon_{ij,k}\varepsilon_{lm,n}/2. \tag{1}$$

Here, C_{ijkl} are the components of the classical fourth-rank elasticity tensor, defined as $C_{ijkl} = C_{jikl} = C_{ijlk} = C_{klij} = \lambda\delta_{ij}\delta_{kl} + \mu(\delta_{ik}\delta_{jl} + \delta_{il}\delta_{jk})$; A_{ijklmn} are the components of the sixth-rank tensor with additional material constants of SGE; $\varepsilon_{ij} = (u_{i,j} + u_{j,i})/2$ are the components of the infinitesimal strain tensor; u_i are the components of the displacement vector.

Within the framework of simplified SGE [1, 13], the components of the tensor A_{ijklmn} are defined as

$$\mathrm{A}_{ijklmn} = \mathrm{A}_{jiklmn} = \mathrm{A}_{ijkmln} = \mathrm{A}_{lmnijk} = l^2\mathrm{C}_{ijlm}\delta_{kn},$$

where l is a length scale parameter with the dimension of length and the only additional material constant of the simplified theory. When the length scale parameter is zero, the formulation of classical elasticity theory is obtained.

Within the framework of classical SGE, the constitutive relations have the form:

– for the stress components

$$\tau_{ij} = \tau_{ji} = \frac{\partial w}{\partial \varepsilon_{ij}} = \mathrm{C}_{ijkl}\varepsilon_{kl} = \lambda\delta_{ij}\varepsilon_{kk} + 2\mu\varepsilon_{ij}; \tag{2}$$

– for the double-stress components

$$\mu_{ijk} = \mu_{jik} = \frac{\partial w}{\partial \varepsilon_{ij,k}} = A_{ijklmn}\varepsilon_{lm,n} = l^2 C_{ijlm}\varepsilon_{lm,k} = l^2\tau_{ij,k}, \tag{3}$$

which in the simplified theory are derivatives of the classical stresses multiplied by the square of the length scale parameter.

It should be noted that the method for implementing numerical solutions described below allows the use, within SGE, of models with more general constitutive relations, including the Mindlin formulation with five additional independent material constants (length scale parameters) [18, 43].

2.2. Variational formulation

From relations (1)–(3), the expression for the variation of the total strain energy of a body occupying a domain Ω, with boundary $\partial\Omega$ and edges $\partial\partial\Omega$ is obtained:

$$\delta W = \int\limits_{\Omega} \delta w dv = \int\limits_{\Omega} (\tau_{ij}\delta\varepsilon_{ij} + \mu_{ijk}\delta\varepsilon_{ij,k}) dv.$$

Accordingly, the variation of the work of external forces is represented as [18]

$$\delta W^{ext} = \int\limits_{\Omega} b_i \delta u_i dv + \int\limits_{\partial\Omega} \bar{t}_i \delta u_i ds + \int\limits_{\partial\Omega} \bar{m}_i n_k \delta u_{i,k} ds + \int\limits_{\partial\partial\Omega} \bar{s}_i \delta u_i dl$$

and includes the prescribed components of the problem parameters: b_i is the body force, $\bar{t}_i$ is the traction vector, $\bar{m}_i$ is the double-traction vector, n_i are the components of the unit normal to the boundary $\partial\Omega$, and $\bar{s}_i$ is the line-force vector acting on the edge $\partial\partial\Omega$.

Then the variational formulation of the problem takes the following form:

$$\int\limits_{\Omega} (\tau_{ij}\delta\varepsilon_{ij} + \mu_{ijk}\delta\varepsilon_{ij,k}) dv = \int\limits_{\Omega} b_i \delta u_i dv + \int\limits_{\partial\Omega} \bar{t}_i \delta u_i ds + \int\limits_{\partial\Omega} \bar{m}_i n_k \delta u_{i,k} ds + \int\limits_{\partial\partial\Omega} \bar{s}_i \delta u_i dl,$$

which corresponds to the following boundary-value problem:

$$\begin{cases} \sigma_{ij,j} + b_i = 0, \quad x_i \in \Omega, \\ t_i = \bar{t}_i \quad \text{or} \quad u_i = \bar{u}_i, \quad x_i \in \partial\Omega, \\ m_i = \bar{m}_i \quad \text{or} \quad u_{i,j} n_j = \bar{g}_i, \quad x_i \in \partial\Omega, \\ s_i = \bar{s}_i \quad \text{or} \quad u_i = \bar{u}_i^e, \quad x_i \in \partial\partial\Omega. \end{cases} \tag{4}$$

Here, $\sigma_{ij} = \tau_{ij} - \mu_{ijk,k}$ are the components of the total stress tensor, and g_i are the components of the normal derivatives of the displacement vector.

It follows from (4) that the SGE boundary-value problem contains additional boundary conditions for double tractions on the body surface or for normal derivatives of the displacement vector, as well as boundary conditions on the body edge. The components of the traction vector on the body surface take the following form:

$$t_i = \sigma_{ij} n_j + D_j(\mu_{ijk} n_k) + (D_l n_l)\mu_{ijk} n_j n_k, \tag{5}$$

where D_i is the surface-gradient operator.

2.3. Finite-element formulation of the SGE problem

Consider the FEM formulation as applied to SGE problems [21, 22]. As in its classical version, the displacement field inside an element is described by the following relation:

$$\mathbf{u} = \begin{Bmatrix} u \\ v \end{Bmatrix} = \mathbf{N}\widehat{\mathbf{u}}, \tag{6}$$

where $\mathbf{N}$ is the matrix of shape functions, $\widehat{\mathbf{u}}$ is the vector of nodal degrees of freedom, and the strains and their gradients are defined as

$$\boldsymbol{\varepsilon} = \begin{Bmatrix} \varepsilon_{11} \\ \varepsilon_{22} \\ 2\varepsilon_{12} \end{Bmatrix} = \mathbf{B}_1\widehat{\mathbf{u}}, \qquad \boldsymbol{\kappa} = \begin{Bmatrix} \varepsilon_{11,1} \\ \varepsilon_{11,2} \\ \varepsilon_{22,1} \\ \varepsilon_{22,2} \\ 2\varepsilon_{12,1} \\ 2\varepsilon_{12,2} \end{Bmatrix} = \mathbf{B}_2\widehat{\mathbf{u}}. \tag{7}$$

Here, $\mathbf{B_1}$ and $\mathbf{B_2}$ are the matrices of the first and second derivatives of the shape functions:

$$\begin{gathered}\mathbf{B}_1=\mathbf{L}_1\mathbf{N},\quad \mathbf{B}_2=\mathbf{L}_2\mathbf{N},\\ \mathbf{L}_1=\begin{pmatrix}\dfrac{\partial}{\partial x} & 0 & \dfrac{\partial}{\partial y}\\ 0 & \dfrac{\partial}{\partial y} & \dfrac{\partial}{\partial x}\end{pmatrix}^{\mathrm{T}},\\ \mathbf{L}_2=\begin{pmatrix}\dfrac{\partial^2}{\partial x^2} & \dfrac{\partial^2}{\partial x\partial y} & 0 & 0 & \dfrac{\partial^2}{\partial y\partial x} & \dfrac{\partial^2}{\partial y^2}\\ 0 & 0 & \dfrac{\partial^2}{\partial y\partial x} & \dfrac{\partial^2}{\partial y^2} & \dfrac{\partial^2}{\partial x^2} & \dfrac{\partial^2}{\partial x\partial y}\end{pmatrix}^{\mathrm{T}}.\end{gathered} \tag{8}$$

The constitutive relations in matrix form take the following form:

$$\boldsymbol{\tau}=\begin{Bmatrix}\tau_{11}\\ \tau_{22}\\ \tau_{12}\end{Bmatrix}=\mathbf{C}\boldsymbol{\varepsilon}=\mathbf{C}\mathbf{B}_1\widehat{\mathbf{u}},\quad \boldsymbol{\mu}=\begin{Bmatrix}\mu_{111}\\ \mu_{112}\\ \mu_{221}\\ \mu_{222}\\ \mu_{121}\\ \mu_{122}\end{Bmatrix}=\mathbf{A}\boldsymbol{\kappa}=\mathbf{A}\mathbf{B}_2\widehat{\mathbf{u}}, \tag{9}$$

where

$$\begin{gathered}\mathbf{C}=\begin{pmatrix}\lambda+2\mu & \lambda & 0\\ \lambda & \lambda+2\mu & 0\\ 0 & 0 & \mu\end{pmatrix},\\ \mathbf{A}=l^2\begin{pmatrix}\lambda+2\mu & 0 & \lambda & 0 & 0 & 0\\ 0 & \lambda+2\mu & 0 & \lambda & 0 & 0\\ \lambda & 0 & \lambda+2\mu & 0 & 0 & 0\\ 0 & \lambda & 0 & \lambda+2\mu & 0 & 0\\ 0 & 0 & 0 & 0 & \mu & 0\\ 0 & 0 & 0 & 0 & 0 & \mu\end{pmatrix}.\end{gathered} \tag{10}$$

Here, λ and μ are the Lamé constants. From relations (6)–(10), the variational formulation in matrix form is obtained:

$$\left(\int\limits_{\Omega}\left(\mathbf{B}_1^{\mathrm{T}}\mathbf{C}\mathbf{B}_1+\mathbf{B}_2^{\mathrm{T}}\mathbf{A}\mathbf{B}_2\right)d\Omega\right)\widehat{\mathbf{u}}=\int\limits_{\Omega}\mathbf{N}^{\mathrm{T}}\mathbf{b}d\Omega+\int\limits_{\partial\Omega}\mathbf{N}^{\mathrm{T}}\mathbf{t}ds+\int\limits_{\partial\Omega}\overline{\mathbf{N}}^{\mathrm{T}}\mathbf{m}ds+\int\limits_{\partial\partial\Omega}\mathbf{N}^{\mathrm{T}}\mathbf{s}dl. \tag{11}$$

The variational formulation (11) corresponds to the SGE problem in FEM terms,

$$\mathbf{K}\widehat{\mathbf{u}}=\mathbf{f}, \tag{12}$$

provided that:

$$\begin{gathered}\mathbf{K}=\int\limits_{\Omega}\left(\mathbf{B}_1^{\mathrm{T}}\mathbf{C}\mathbf{B}_1+\mathbf{B}_2^{\mathrm{T}}\mathbf{A}\mathbf{B}_2\right)d\Omega,\\ \mathbf{f}=\int\limits_{\Omega}\mathbf{N}^{\mathrm{T}}\mathbf{b}d\Omega+\int\limits_{\partial\Omega}\mathbf{N}^{\mathrm{T}}\mathbf{t}ds+\int\limits_{\partial\Omega}\overline{\mathbf{N}}^{\mathrm{T}}\mathbf{m}ds+\int\limits_{\partial\partial\Omega}\mathbf{N}^{\mathrm{T}}\mathbf{s}dl.\end{gathered}$$

The residual vector used to verify the accuracy of the obtained solution (12) is calculated as

$$\mathbf{r}=\int\limits_{\Omega}\left(\mathbf{B}_1^{\mathrm{T}}\boldsymbol{\tau}+\mathbf{B}_2^{\mathrm{T}}\boldsymbol{\mu}\right)dv-\mathbf{f}.$$

3. Modified finite elements

Standard finite elements are capable of realizing all the advantages of SGE in solving various problems. However, the use of such elements requires substantial mesh refinement near concentrators to correctly determine the displacement and strain fields, which increases the computational cost. The enriched elements considered in this section employ asymptotic functions to describe the fields of the SGE problem parameters near the crack tip [22]; they make it possible to construct a coarser mesh near concentrators for stress determination and also to calculate the amplitude coefficients of the asymptotic solution. The latter make it possible to use the mathematical tools of fracture mechanics in crack analysis, in particular to compute the J-integral. However, different types of concentrators require different asymptotic functions. Therefore, at this stage, the present work discusses enriched elements only for plane crack problems (in modes I and II).

3.1. Standard elements

Standard three-node finite elements have 36 degrees of freedom (12 at each node). These include not only nodal displacements but also their first and second derivatives:

$$\widehat{\mathbf{u}} = \{u_1, u_{1,x}, u_{1,y}, u_{1,xx}, u_{1,xy}, u_{1,yy}, v_1, v_{1,x}, v_{1,y}, v_{1,xx}, v_{1,xy}, v_{1,yy}, u_2 ... v_{2,yy}, u_3 ... v_{3,yy}\}^{\mathrm{T}}.$$

To realize C^1-continuity, complete fifth-order polynomials in L-coordinates, originally developed for plate-bending problems [44], are used as shape functions. The shape-function matrix $\mathbf{N}$ has the following structure:

$$\mathbf{N} = \begin{bmatrix} N_1 ... N_6 & 0...0 & N_7 ... N_{12} & 0...0 & N_{13} ... N_{18} & 0...0 \\ 0...0 & N_1 ... N_6 & 0...0 & N_7 ... N_{12} & 0...0 & N_{13} ... N_{18} \end{bmatrix}.$$

3.2. Enriched elements

When enriched elements are used, the displacement field is represented as follows [22]:

$$u = \sum_{i=1}^{18} \hat{u}_i N_i + \sum_{n=1}^{4} K_n Q^*_{1n},$$
$$v = \sum_{i=1}^{18} \hat{v}_i N_i + \sum_{n=1}^{4} K_n Q^*_{2n},$$

where

$$Q^*_{in} = Q_{in} - \sum_{j=1}^{3} Q^{(j)}_{in} N^{(0)}_j - \sum_{j=1}^{3} \frac{\partial Q^{(j)}_{in}}{\partial x} N^{(1)}_j - \sum_{j=1}^{3} \frac{\partial Q^{(j)}_{in}}{\partial y} N^{(2)}_j.$$

In these relations, the second sums are asymptotic crack solutions within SGE, and K_n are amplitude coefficients. Thus, enriched finite elements have 40 degrees of freedom, and the vector of nodal degrees of freedom takes the following form:

$$\widehat{\mathbf{u}} = \{u_1, u_{1,x}, u_{1,y}, u_{1,xx}, u_{1,xy}, u_{1,yy}, v_1, v_{1,x}, v_{1,y}, v_{1,xx}, v_{1,xy}, v_{1,yy}, u_2 ... v_{2,yy}, u_3 ... v_{3,yy}, K_1, K_2, K_3, K_4\}^{\mathrm{T}}. \quad (13)$$

The form of expression (13) is dictated by the aim of preserving C^1-continuity at the element nodes and corresponds to classical element enrichment [36].

The functions Q_{in}, which are asymptotic solutions, are defined as follows:

$$Q_{11}=\frac{1}{4\mu}r^{3/2}\cos\frac{\theta}{2}(-4-2\eta+2(1+2\eta)\cos\theta),$$
$$Q_{12}=\frac{1}{4\mu}r^{3/2}\cos\frac{\theta}{2}\left(\frac{7+10\eta}{3}-\frac{14+8\eta}{3}\cos\theta-\cos2\theta\right),$$
$$Q_{13}=\frac{1}{4\mu}r^{3/2}\sin\frac{\theta}{2}(5-4\eta+4(4+\eta)\cos\theta+3\cos2\theta),$$
$$Q_{14}=\frac{1}{4\mu}r^{3/2}\sin\frac{\theta}{2}(1+2\cos\theta),$$
$$Q_{21}=\frac{1}{4\mu}r^{3/2}\sin\frac{\theta}{2}(-4+2\eta-2(1-2\eta)\cos\theta),$$
$$Q_{22}=\frac{1}{4\mu}r^{3/2}\sin\frac{\theta}{2}\left(\frac{7-2\eta}{3}+\frac{14+8\eta}{3}\cos\theta-\cos2\theta\right),$$
$$Q_{23}=\frac{1}{4\mu}r^{3/2}\cos\frac{\theta}{2}(-5-12\eta+4(4+3\eta)\cos\theta-3\cos2\theta),$$
$$Q_{24}=\frac{1}{4\mu}r^{3/2}\cos\frac{\theta}{2}(1-2\cos\theta).$$

Here, r and θ are polar coordinates, $\eta=3-4\nu$, where ν is Poisson's ratio.

3.3. Numerical integration

For numerical integration of the three-node elements, reduced Gaussian quadrature with 13 integration points was used (Fig. 1). As shown in [22], this is sufficient to obtain accurate results on meshes composed of both standard and enriched elements.

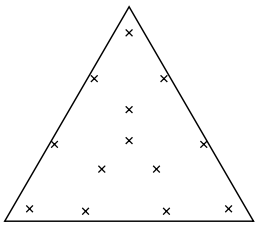


Fig. 1. Location of the integration points

3.4. Implementation in Abaqus/CAE

To solve the SGE problem by FEM in the commercial Abaqus/CAE package, its solver was supplemented with a user element subroutine (UEL) written in Fortran [45] and containing a description of the elements used for discretization. A user interface in the form of a Python plugin was also created to automate preparation of the input file with the selected type of modified element at the crack tip (standard or enriched), with the length scale parameter and boundary conditions. The interaction scheme of Abaqus/CAE, UEL, and the user interface is shown in Fig. 2. The numbered arrows indicate the steps and their directions: 1, 2 — user specification of the input data; 3 — transfer of the mesh, classical boundary conditions, applied loads, and node and element sets; 4 — generation and transfer to the solver of an input file defining the user elements and boundary conditions; 5 — transfer of data for calculating the stiffness matrix of an individual element and the internal-force vector; 6 — transfer of the element stiffness matrix and the internal-force vector for assembling the global stiffness matrix, as well as transfer of stress, strain, and gradient values; 7 — generation of the results file for subsequent visualization and analysis.

The mandatory (interface) part of the UEL [45], which describes the input and output information about variables and arrays that the Abaqus/Standard solver sends to and receives from the UEL, is shown in Fig. 3.

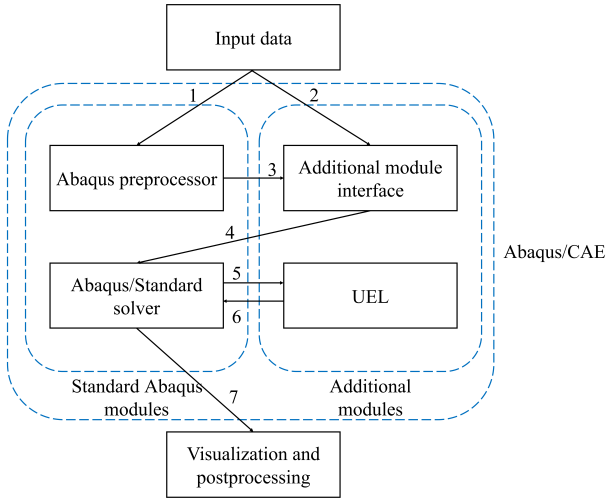


Fig. 2. Interaction scheme of Abaqus/CAE, UEL, and the user interface

```
SUBROUTINE UEL(RHS,AMATRX,SVARS,ENERGY,NDOFEL,NRHS,NSVARS,
1 PROPS,NPROPS,COORDS,MCRD,NNODE,U,DU,V,A,JTYPE,TIME,DTIME,
2 KSTEP,KINC,JELEM,PARAMS,NDLOAD,JDLTYP,ADLMAG,PREDEF,NPREDF,
3 LFLAGS,MLVARX,DDLMAG,MDLOAD,PNEWDT,JPROPS,NJPROP,PERIOD)
C
INCLUDE 'ABA_PARAM.INC'
C
DIMENSION RHS(MLVARX,*),AMATRX(NDOFEL,NDOFEL),PROPS(*),
1 SVARS(*),ENERGY(8),COORDS(MCRD,NNODE),U(NDOFEL),
2 DU(MLVARX,*),V(NDOFEL),A(NDOFEL),TIME(2),PARAMS(*),
3 JDLTYP(MDLOAD,*),ADLMAG(MDLOAD,*),DDLMAG(MDLOAD,*),
4 PREDEF(2,NPREDF,NNODE),LFLAGS(*),JPROPS(*)

user coding to define RHS, AMATRX, SVARS, ENERGY, and PNEWDT

RETURN
END
```

Fig. 3. UEL subroutine interface

To account for the functional of an individual FE when discretizing the computational domain of the SGE problem, the main part of the UEL calculates its characteristic arrays: RHS, which contains the element contribution to the residual vector (external minus internal forces in the usual static procedure); AMATRX, which represents its contribution to the Jacobian (stiffness) matrix. For this purpose, Abaqus/Standard passes the element nodal coordinates, displacement vector, material properties, and other data to the UEL.

In this work, the UEL subroutine is implemented so as to describe both standard and enriched elements, depending on the element type assigned in the input file. This makes it possible to use both types in a single calculation. The flowchart of the UEL subroutine and the user interface are shown in Fig. 4. The user interface allows properties, including the length scale parameter, as well as additional boundary conditions arising in SGE, to be specified. After initialization, an input file in .inp format is generated, containing commands that declare the type of user elements, properties, and boundary conditions.

4. Numerical results

The results of solving the central-crack problem using standard elements (in modes I, II, and mixed mode) and enriched elements (in modes I and II) are presented below.

4.1. Solution with standard elements

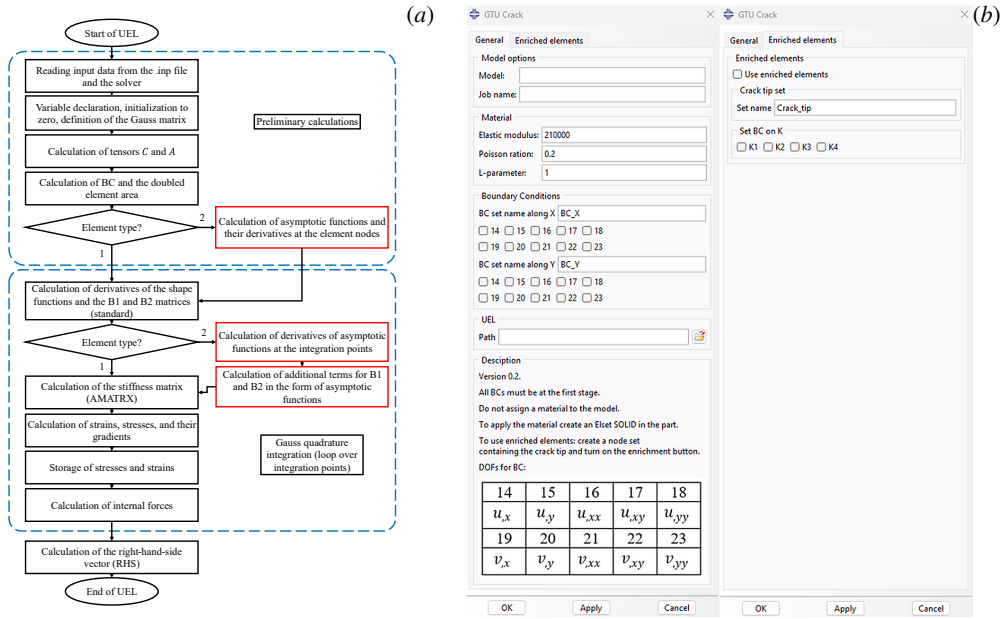


Fig. 4. Flowchart of the UEL subroutine (*a*); user-interface plugin (*b*)

A problem is considered for a crack of length $2a$ in an infinite domain subjected to tensile (mode I) and shear (mode II) loading P_0 under plane-strain conditions. The corresponding FE models are shown in Fig. 5. Owing to the symmetry of the problem in mode I and antisymmetry in mode II, only 1/4 of the domain of size $L \times L$ is considered. Several crack lengths $a/l = \{2.5, 5.0, 10, 15, 20\}$ were investigated. Based on mesh convergence (Fig. 6), the element size near the crack tip was chosen as $s/l = 0.01$. For clarity, the figure combines plots of the maximum stresses at the crack tip calculated by FEM within the framework of SGE and using the classical FEM formulation. The mesh contained a total of 5000 elements and 2600 nodes.

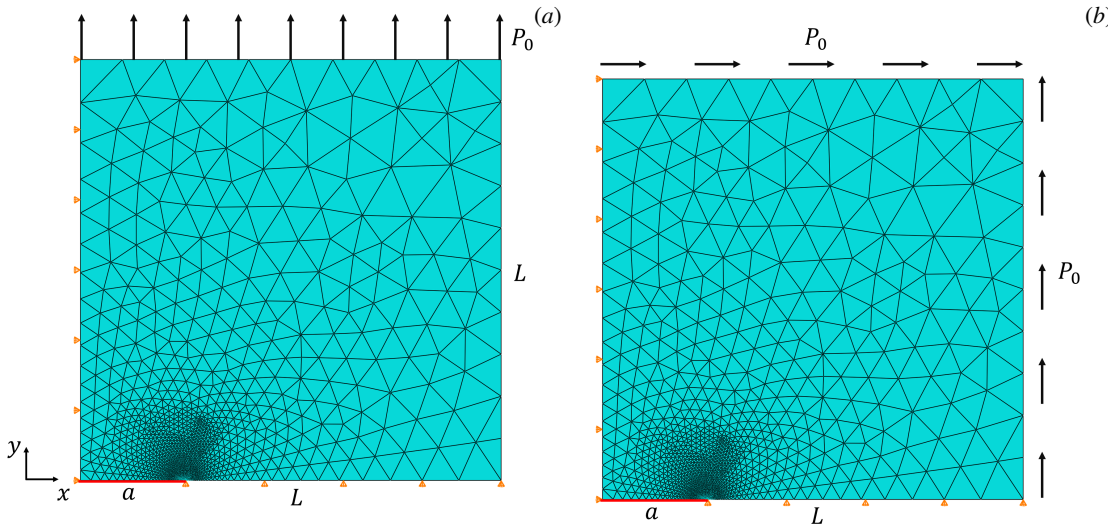


Fig. 5. Finite-element model: mode I (*a*); mode II (*b*)

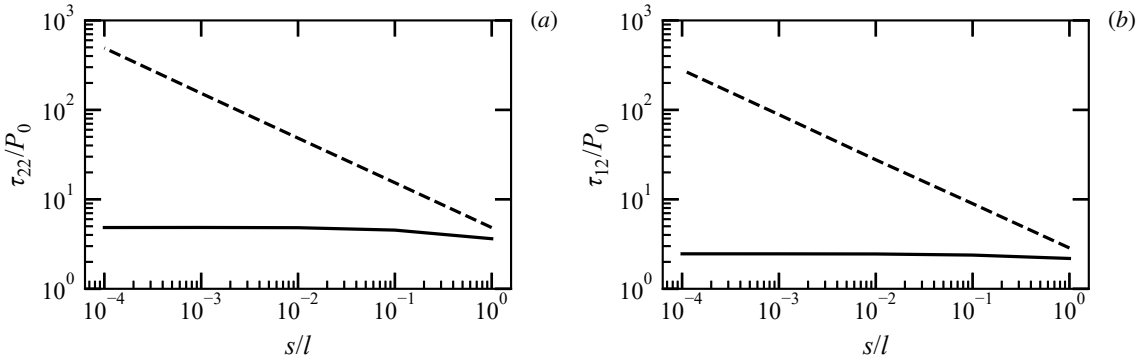


Fig. 6. Maximum relative stresses at the crack tip as a function of the relative element size at the crack tip s/l for the classical solution (dashed line) and the solution within SGE (solid line): mode I (*a*); mode II (*b*)

Because the SGE formulation is used, in addition to displacement boundary conditions, constraints are imposed on the first and second displacement derivatives to ensure symmetry for mode I and antisymmetry for mode II:
– symmetry boundary conditions

$$\begin{aligned} &x=-a,\ 0\leqslant y\leqslant L: \quad u=0,\ u_y=0,\ u_{yy}=0,\ v_x=0,\ v_{xy}=0,\\ &a\leqslant x\leqslant L,\ y=0: \quad v=0,\ v_x=0,\ v_{xx}=0,\ u_y=0,\ u_{xy}=0; \end{aligned}$$

– antisymmetry boundary conditions

$$\begin{aligned} &x=-a,\ 0\leqslant y\leqslant L: \quad v=0,\ v_y=0,\ v_{yy}=0,\ u_x=0,\ u_{xy}=0,\\ &a\leqslant x\leqslant L,\ y=0: \quad u=0,\ u_x=0,\ u_{xx}=0,\ v_y=0,\ v_{xy}=0. \end{aligned}$$

The main advantage of applying a C^1-continuous FEM in the SGE formulation is the use of the fundamental property of smoothing singular solutions of classical elasticity theory, that is, transferring them into the class of regular solutions. This is demonstrated by the stress plots in Fig. 7. A consequence of the SGE solution, in contrast to classical theory, is the presence of nonzero stresses on the crack faces. They arise due to the more complex boundary conditions (5) and serve as an equivalent of the forces introduced in the Barenblatt theory [27, 46] to eliminate the singularity.

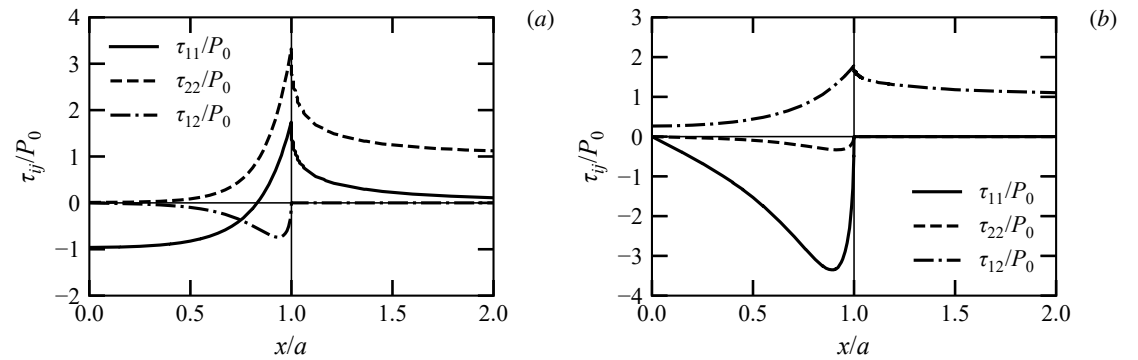


Fig. 7. Relative stresses along the crack line $y=0$ at $a/l=10$ as a function of the relative coordinate x/a: mode I (*a*); mode II (*b*)

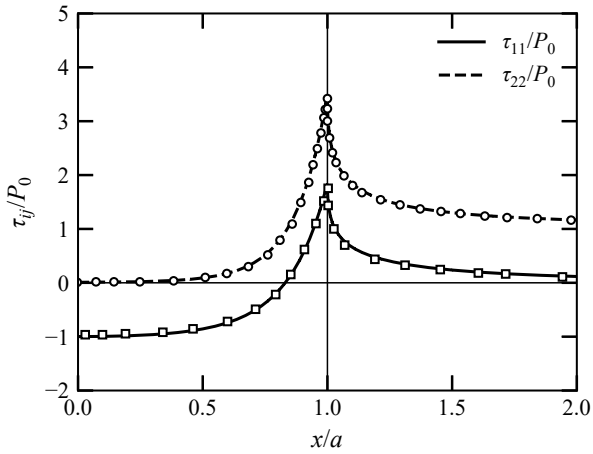


Fig. 8. Stresses along the crack line $y=0$ at $a/l=10$: solid lines – authors' solution, markers – solution from [21]

In Fig. 8, in addition to the authors' data, the calculation data from [21] are presented for comparison; they confirm that the implementation of the user subroutines is correct (the solutions coincide).

The problem was also solved for a crack under mixed-mode conditions (Fig. 9). The external load and material properties were taken to be the same as in the previous calculations. Based on the computed data, curves of the relative maximum principal stresses σ_1/P_0 and the dependence of the angle of the planes on which they act on the crack-orientation angle were constructed (Fig. 10). This result, on the one hand, confirms the possibility of obtaining, for cracks, the data required to use classical strength criteria, as demonstrated in [27], and, on the other hand, shows that this approach is an alternative to the tools of linear fracture mechanics and provides a unification of strength-analysis approaches.

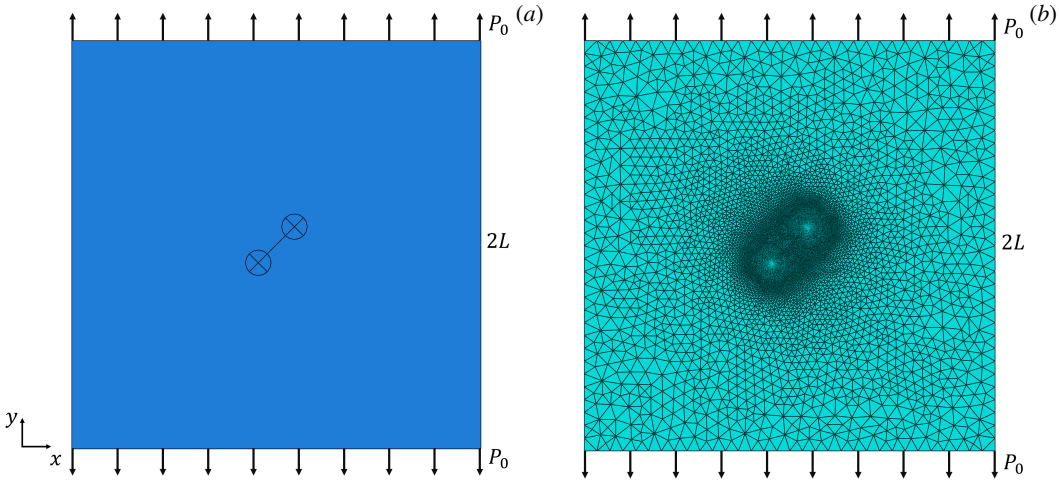


Fig. 9. Finite-element model of a crack oriented at an angle $\beta=45°$, under mixed-mode loading

4.2. Solution with enriched elements

When solving the crack problem in modes I and II with enriched elements, 1/4 of the domain of size $L\times L$ under load P_0 was also considered. The ratio of crack length to L was varied as $a/L=\{0.02,0.05,0.1,0.25,0.5\}$, and the length scale parameter was $l/L=\{0.05,0.1,0.2\}$. To obtain a correct result, a mesh consisting of a prescribed number of enriched elements of the same size was generated around the crack (Fig. 11); the remaining elements of the model were standard. Mesh convergence was achieved for the amplitude coefficients as the number of elements around the crack tip was increased, as well as faster convergence in terms of the maximum stresses (see Fig. 12).

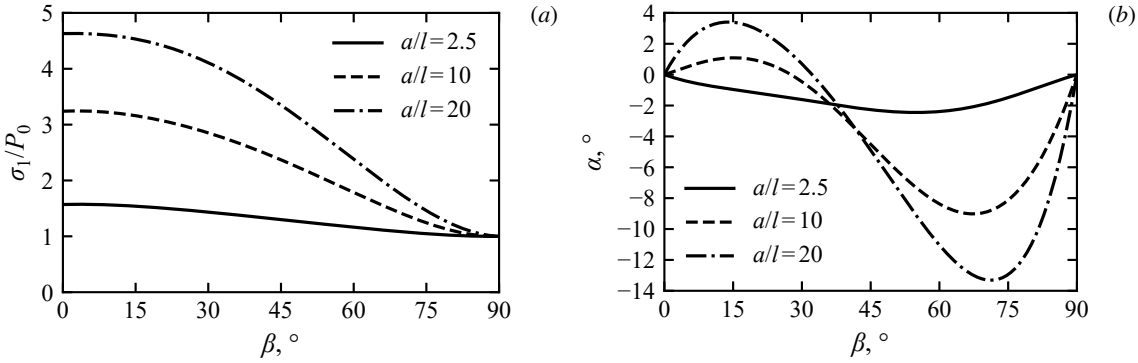


Fig. 10. Dependences of the relative maximum principal stresses σ_1/P_0 (*a*) and the angle α of the planes on which they act (*b*) on the crack-orientation angle β

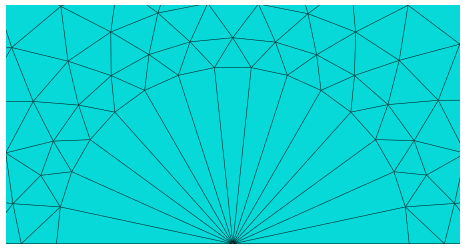


Fig. 11. Crack model using enriched elements

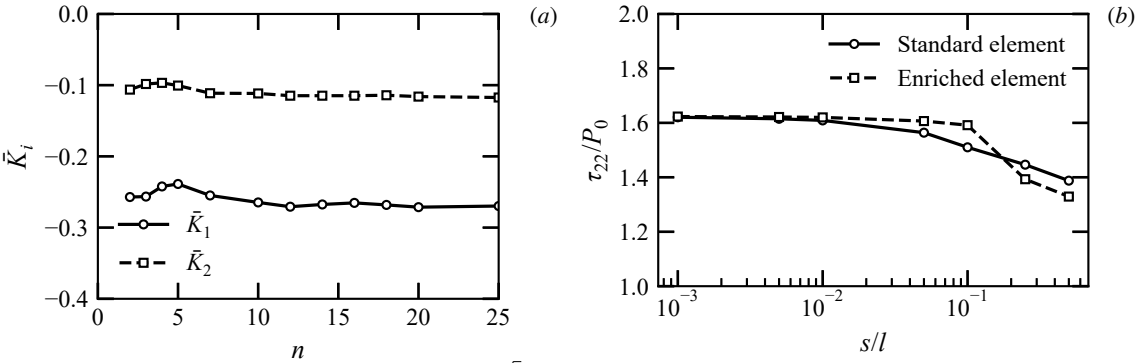


Fig. 12. Relative amplitude coefficients $\bar{K}_i = K_i/(P_0/\sqrt{l})$ as a function of the number of elements n around the crack tip (*a*); relative maximum stresses for mode I as functions of the relative element size s/l (*b*)

Figure 13 shows the stresses in modes I and II for one of the crack sizes; for the same problem, the stresses obtained using only standard elements are also given. At the crack tip, the size of the standard element was $s/L=0.001$, whereas for enriched elements it was an order of magnitude larger: $s/L=0.01$. As can be seen, the solutions coincide completely.

Figure 14 contains plots of the maximum stresses as functions of crack size and scale-parameter value. As the crack size decreases, τ_{11} for mode I tends to zero, whereas τ_{22} for mode I and τ_{12} for mode II approach the applied stress P_0. For larger values of the length scale parameter, these latter stresses remain close to P_0 over a wider range of crack lengths. This indicates that, at larger values of the length scale parameter, the material becomes less sensitive to small defects. Conversely, as the length scale parameter decreases, stress concentration increases even for small crack sizes. As the length scale parameter tends to zero, the stresses grow without bound, which corresponds to the classical solution of the elasticity problem.

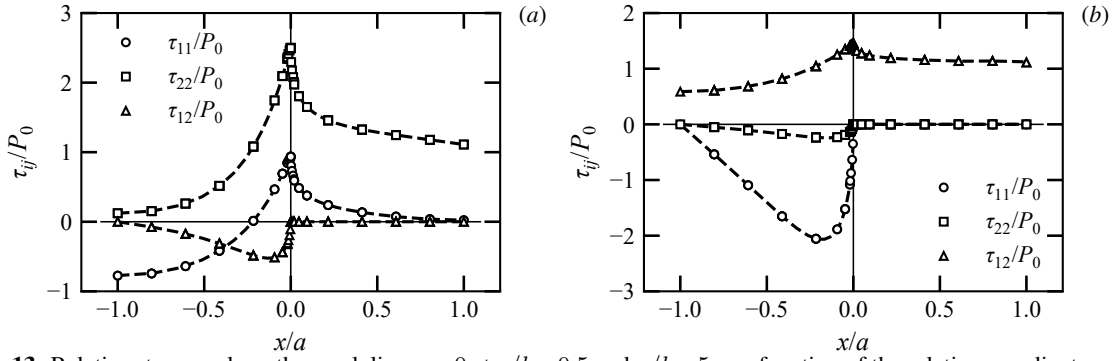


Fig. 13. Relative stresses along the crack line $y = 0$ at $a/l = 0.5$ and $a/l = 5$ as a function of the relative coordinate x/a; markers denote solutions with enriched elements, dashed lines denote solutions with standard elements: mode I (*a*); mode II (*b*)

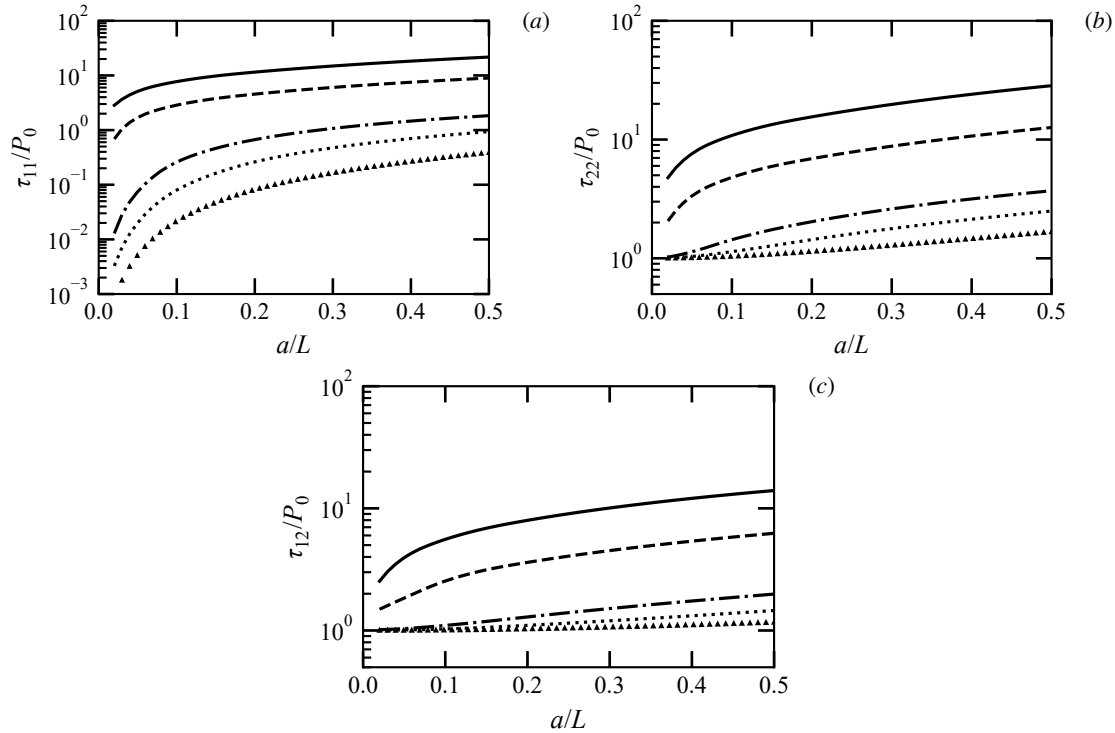


Fig. 14. Maximum stresses at the crack tip as functions of crack length a/L for different values of the length scale parameter l/L: 0.001 (solid line), 0.005 (dashed line), 0.05 (dash-dotted line), 0.1 (dotted line), 0.2 (line with triangles); mode I, τ_{11}/P_0 (*a*); mode I, τ_{22}/P_0 (*b*); mode II, τ_{12}/P_0 (*c*)

4.3. Amplitude coefficients

The use of enriched elements makes it possible to determine the values of the amplitude coefficients of the asymptotic solutions normalized by $P_0/\sqrt{l}$. Their absolute values are presented in Fig. 15 (according to the solution, the amplitude coefficients have a negative sign). This, in turn, opens the possibility of using mathematical estimates from linear fracture mechanics, such as the J-integral. However, it should be noted that the amplitude coefficients obtained within FE models do not correspond to the classical SIFs and have units of $\mathrm{Pa}/\sqrt{\mathrm{m}}$. As can be seen from the plots, as the crack size decreases, the magnitude of the amplitude coefficients also decreases, indicating a reduction in stress concentration at the crack tip. As the length scale parameter decreases, the opposite effect is observed: the absolute values of the amplitude coefficients increase.

In [22], expressions for the J-integral for modes I and II were obtained; these are calculated using the amplitude coefficients found from the solution of the problem in the SGE formulation:

$$J_I = \frac{1+\eta}{8\mu}\pi l^2\Big((3K_1+K_2)^2+8K_2^2(\eta+2)\Big),$$
$$J_{II} = \frac{1+\eta}{8\mu}\pi l^2\left(72K_3^2(\eta+2)+\frac{9K_4^2}{4(\eta^2-1)}\right).$$

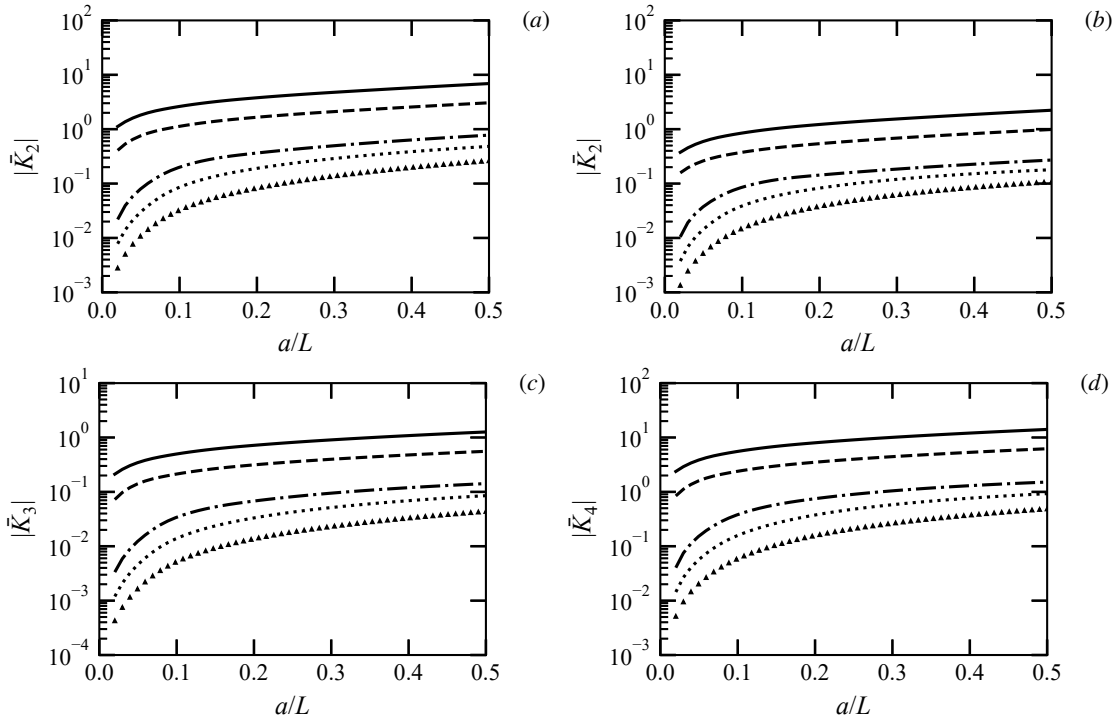


Fig. 15. Absolute values of the normalized amplitude coefficients of the asymptotic solutions as functions of the relative crack length a/L for different values of the length scale parameter l/L: 0.001 (solid line), 0.005 (dashed line), 0.05 (dash-dotted line), 0.1 (dotted line), 0.2 (line with triangles); mode I, $\bar{K}_1$ (*a*), mode I, $\bar{K}_2$ (*b*), mode II, $\bar{K}_3$ (*c*), mode II, $\bar{K}_4$ (*d*)

Figure 16 presents plots of the relative values J/J_0, where $J_0 = [(1+\eta)/(8\mu)]\Big(P_0\sqrt{\pi L/40}\Big)^2$, for different values of the length scale parameter l as functions of the relative crack length a/L. It can be seen from the figures that, as the length scale parameter decreases, the plot of the relative J-integral tends to the classical solution $J = [(1+\eta)/(8\mu)]{K_I}^2$ (here K_I is the classical SIF), but, unlike the classical solution, values close to zero are obtained at a nonzero crack size. This result indicates that enriched elements can be used to identify the length scale parameter when processing experimental data.

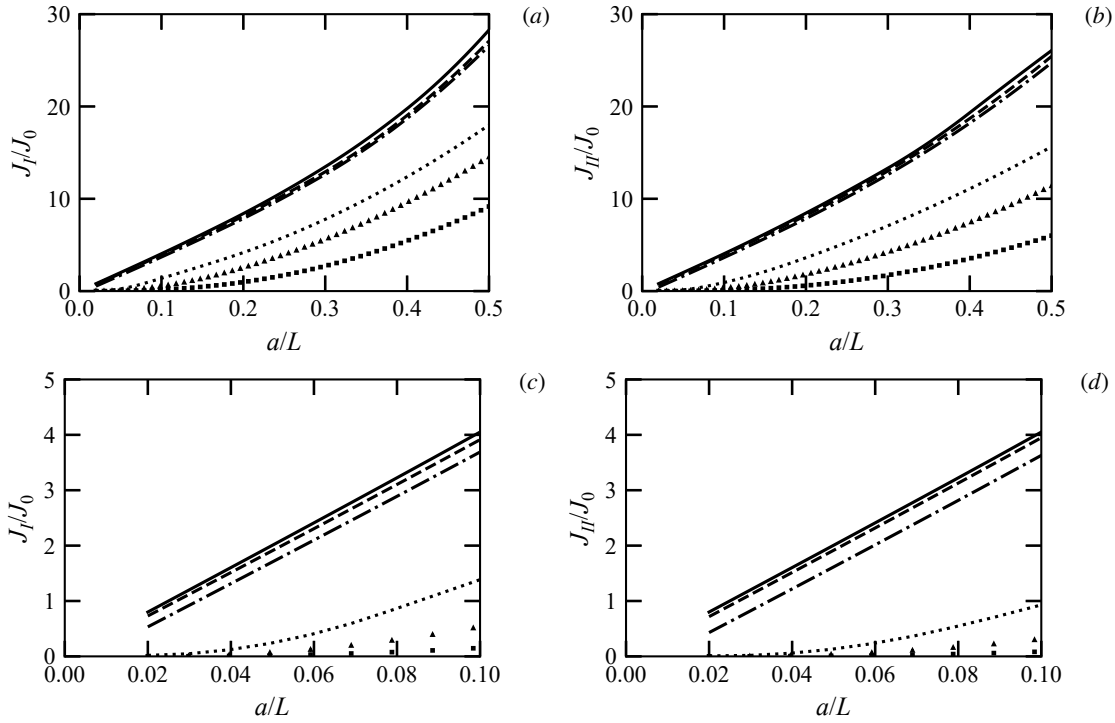


Fig. 16. Values of the relative J-integral in the classical solution (solid line) and for different values of the length scale parameter l/L: 0.001 (dashed line), 0.005 (dash-dotted line), 0.05 (dotted line), 0.1 (line with triangles), 0.2 (line with squares); mode I (*a*); mode II (*b*), mode I (*c*), mode II (*d*)

5. Conclusions

Mode I, mode II, and mixed-mode crack problems were solved in the commercial finite-element analysis software package Abaqus/CAE, supplemented with the authors' user element subroutine (UEL), which describes two types of finite elements, and a user interface in the form of a plugin for automating input-file generation.

The main advantages of solving the problem within SGE using standard and enriched elements were demonstrated. Their application makes it possible to eliminate singularities at the crack tip, obtain equilibrium crack opening, and correctly account for small defects. Finite stress values at the crack tip make it possible to assess the strength of structures based on both existing and newly developed criteria.

Calculations with enriched elements show that they are preferable in terms of computational cost owing to their faster convergence. In addition, determination of the amplitude coefficients becomes available, and these coefficients can be used to compute the J-integral. However, at the present stage their use is possible only for crack analysis.

The presented results may be useful in experimental fracture mechanics for unifying methods of identifying additional SGE parameters on the basis of standard tests.

The research was supported by the Russian Science Foundation (project No. 22-79-10228-П); information about the project is available on the Foundation's official website.

References

1. *Askes H., Aifantis E.C.* Gradient elasticity in statics and dynamics: An overview of formulations, length scale identification procedures, finite element implementations and new results. International Journal of Solids and Structures. 2011. Vol. 48. P. 1962–1990. DOI: 10.1016/j.ijsolstr.2011.03.006
2. *Bärnkopf E., Kövesdi B., Dunai L.* Investigation of Stress Concentration Zones in FEM-Based Design of Welded Plated Structures. Buildings. 2023. Vol. 13. 1057. DOI: 10.3390/buildings13041057
3. *Solyaev Y.O.* Neklassicheskiye masshtabnyye effekty v prikladnykh modelyakh gradiyentnoy teorii uprugosti i elektrouprugosti:

PhD Dissertation in Physical and Mathematical Sciences / Solyaev Yury Olegovich. Moscow: Institute of Applied Mechanics of the Russian Academy of Sciences, 2022. 295 p.

4. *Sinclair G.B.*, *Beisheim J.R.*, *Kardak A.A.* On the Detection of Stress Singularities in Finite Element Analysis. Journal of Applied Mechanics. 2019. Vol. 86. 021005. DOI: 10.1115/1.4041766
5. *Korepanov V.V.*, *Matveenko V.P.*, *Fedorov A. Yu.*, *Shardakov I.N.* Numerical analysis of singular solutions of two-dimensional problems of asymmetric elasticity. Mechanics of Solids. 2013. Vol. 48. P. 397–404. DOI: 10.3103/S0025654413040067
6. *Matveenko V.P.*, *Fedorov A.Y.*, *Galkina E.B.* Numerical investigation of stress concentration at the tip of the V-notch partially filled with material. Computational Continuum Mechanics. 2022. Vol. 15, no. 3. P. 333–342. DOI: 10.7242/1999-6691/2022.15.3.25
7. *Valvo P.S.* A further step towards a physically consistent virtual crack closure technique. International Journal of Fracture. 2015. Vol. 192. P. 235–244. DOI: 10.1007/s10704-015-0007-4
8. *Krueger R.* Virtual crack closure technique: History, approach, and applications. Applied Mechanics Reviews. 2004. Vol. 57. P. 109–143. DOI: 10.1115/1.1595677
9. *Lekhnitskii S.G.* Anisotropic Plates. Gordon and Breach Science Publishers, 1968. 534 p.
10. *Moes N.*, *Dolbow J.*, *Belytschko T.* A finite element method for crack growth without remeshing. International Journal for Numerical Methods in Engineering. 1999. Vol. 46. P. 131–150. DOI: 10.1002/(SICI)1097-0207(19990910)46:1<131::AID-NME726>3.3.CO;2-A
11. *Ahmed A.* eXtended Finite Element Method (XFEM) - Modeling arbitrary discontinuities and Failure analysis: Dissertation for the Master Degree / Ahmed Awais. 2009. 196 p.
12. *Diehl T.* Modeling Surface-Bonded Structures with ABAQUS Cohesive Elements: Beam-Type Solutions. Abaqus User's Conference Proceedings. 2005. P. 89–115.
13. *Aifantis E.C.* On the role of gradients in the localization of deformation and fracture. International Journal of Engineering Science. 1992. Vol. 30. P. 1279–1299. DOI: 10.1016/0020-7225(92)90141-3
14. *Cauchy L.* Note sur l'équilibre et les mouvements vibratoires des corps solides. Comptes Rendus de l'Académie des Sciences. 1851. Vol. 32. P. 323–326.
15. *Kunin I.A.* Teoriya uprugikh sred s mikrostrukturoy: nelokal'naya teoriya uprugosti. Moscow: Nauka, 1975. 415 p.
16. *Aero E.L.*, *Kuvshinskii E.V.* Osnovnyye uravneniya teorii uprugosti sred s vrashchatel'nym vzaimodeystviyem chastits. Fizika Tverdogo Tela. 1960. Vol. 2, no. 7. P. 1399–1409.
17. *Levin V.M.* The relation between mathematical expectations of stress and strain tensors in elastic microheterogeneous media. Journal of Applied Mathematics and Mechanics. 1971. Vol. 35, no. 4. P. 694–701. DOI: 10.1016/0021-8928(71)90064-5
18. *Mindlin R.D.* Micro-structure in linear elasticity. Archive for Rational Mechanics and Analysis. 1964. Vol. 16. P. 52–78. DOI: 10.1007/BF00248490
19. *Toupin R.A.* Elastic materials with couple-stresses. Archive for Rational Mechanics and Analysis. 1962. Vol. 11. P. 385–414. DOI: 10.1007/BF00253945
20. *Green A.E.*, *Rivlin R.S.* Simple force and stress multipoles. Archive for Rational Mechanics and Analysis. 1964. Vol. 16, no. 5. P. 325–353. DOI: 10.1007/BF00281725
21. *Papanicolopulos S.-A.*, *Zervos A.* Numerical solution of crack problems in gradient elasticity. Proceedings of the Institution of Civil Engineers - Engineering and Computational Mechanics. 2010. Vol. 163. P. 73–82. DOI: 10.1680/eacm.2010.163.2.73
22. *Solyaev Y.*, *Dobryanskiy V.* Enriched C^1 Finite Elements for Crack Problems in Simplified Strain Gradient Elasticity. International Journal for Numerical Methods in Engineering. 2025. Vol. 126. e70081. DOI: 10.1002/nme.70081
23. *Vasil'ev V.V.*, *Lurie S.A.*, *Salov V.A.* New Solution to the Problem of a Crack in an Orthotropic Plate under Tension. Mechanics of Solids. 2021. Vol. 56, no. 6. P. 902–910. DOI: 10.3103/S0025654421060200
24. *Vasiliev V.V.*, *Lurie S.A.*, *Salov V.A.* Estimation of the Strength of Plates with Cracks Based on the Maximum Stress Criterion in a Scale-Dependent Generalized Theory of Elasticity. Physical Mesomechanics. 2018. Vol. 21, no. 4. P. 456–462. DOI: 10.1134/S102995991906002X
25. *Vasil'ev V.V.*, *Lur'e S.A.* New Method for Studying the Strength of Brittle Bodies with Cracks. Russian Metallurgy (Metally). 2020. Vol. 2020. P. 291–297. DOI: 10.1134/S0036029520040345

26. *Vasil'ev V.V.*, *Lur'e S.A.* New solution of the plane problem for an equilibrium crack. Mechanics of Solids. 2016. Vol. 51, no. 5. P. 557–561. DOI: 10.3103/S0025654416050071

27. *Vasiliev V.*, *Lurie S.*, *Solyaev Y.* New approach to failure of pre-cracked brittle materials based on regularized solutions of strain gradient elasticity. Engineering Fracture Mechanics. 2021. Vol. 258. 108080. DOI: 10.1016/j.engfracmech.2021.108080

28. *Vasil'ev V.V.*, *Lur'e S.A.* Generalized solution of the problem of a circular membrane loaded by a lumped force. Mechanics of Solids. 2016. Vol. 51, no. 3. P. 334–338. DOI: 10.3103/S0025654416030109

29. *Solyaev Y.*, *Lurie S.*, *Altenbach H.*, *dell'Isola F.* On the elastic wedge problem within simplified and incomplete strain gradient elasticity theories. International Journal of Solids and Structures. 2022. Vol. 239/240. 111433. DOI: 10.1016/j.ijsolstr.2022.111433

30. *Lomakin E.V.*, *Lurie S.A.*, *Rabinskiy L.N.*, *Solyaev Y.O.* Refined Stress Analysis in Applied Elasticity Problems Accounting for Gradient Effects. Doklady Physics. 2019. Vol. 64, no. 12. P. 482–486. DOI: 10.1134/S1028335819120103

31. *Askes H.*, *Susmel L.* Understanding cracked materials: is Linear Elastic Fracture Mechanics obsolete?. Fatigue & Fracture of Engineering Materials & Structures. 2015. Vol. 38. P. 154–160. DOI: 10.1111/ffe.12183

32. *Askes H.*, *Susmel L.* Gradient enriched linear-elastic crack tip stresses to estimate the static strength of cracked engineering ceramics. Fracture and Structural Integrity. 2013. Vol. 7. P. 87–93. DOI: 10.3221/IGF-ESIS.25.13

33. *Bagni C.*, *Askes H.*, *Susmel L.* Gradient-enriched linear-elastic tip stresses to perform the high-cycle fatigue assessment of notched plain concrete. Fracture and Structural Integrity. 2015. Vol. 9. P. 105–110. DOI: 10.3221/IGF-ESIS.33.14

34. *Solyaev Y.O.*, *Sherbakov S.S.*, *Golubkin K.S.*, *et al.* Evaluation of the Length Scale Parameters of Metals Based on Fatigue Tests Data for Samples with Surface Defects. Mechanics of Solids. 2025. Vol. 60. P. 112–127. DOI: 10.1134/S0025654424605305

35. *Adamov A.A.* Homogeneity hypothesis, scale length parameters and edge effect for an isotropic Cosserat continuum. Mekhanika kompozitsionnykh materialov i konstruktsii. 2010. Vol. 16, no. 3. P. 329–346.

36. *Benzley S.E.* Representation of singularities with isoparametric finite elements. International Journal for Numerical Methods in Engineering. 1974. Vol. 8. P. 537–545. DOI: 10.1002/NME.1620080310

37. *Xiao Q.Z.*, *Karihaloo B.L.* An overview of a hybrid crack element and determination of its complete displacement field. Engineering Fracture Mechanics. 2007. Vol. 74. P. 1107–1117. DOI: 10.1016/j.engfracmech.2006.12.022

38. *Stepanova L.V.* Asymptotic Analysis of the Crack Tip Stress Field (Consideration of Higher Order Terms). Numerical Analysis and Applications. 2019. Vol. 12. P. 284–296. DOI: 10.1134/S1995423919030078

39. *Henshell R.D.*, *Shaw K.G.* Crack tip finite elements are unnecessary. International Journal for Numerical Methods in Engineering. 1975. Vol. 9. P. 495–507. DOI: 10.1002/nme.1620090302

40. *Nejati M.*, *Paluszny A.*, *Zimmerman R.W.* On the use of quarter-point tetrahedral finite elements in linear elastic fracture mechanics. Engineering Fracture Mechanics. 2015. Vol. 144. P. 194–221. DOI: 10.1016/j.engfracmech.2015.06.055

41. *Gourgiotis P.A.*, *Georgiadis H.G.* Plane-strain crack problems in microstructured solids governed by dipolar gradient elasticity. Journal of the Mechanics and Physics of Solids. 2009. Vol. 57. P. 1898–1920. DOI: 10.1016/j.jmps.2009.07.005

42. *Solyaev Y.* Higher-order asymptotic crack-tip fields in simplified strain gradient elasticity. Theoretical and Applied Fracture Mechanics. 2024. Vol. 130. 104321. DOI: 10.1016/j.tafmec.2024.104321

43. *Sciarra G.*, *Vidoli S.* Asymptotic Fracture Modes in Strain-Gradient Elasticity: Size Effects and Characteristic Lengths for Isotropic Materials. Journal of Elasticity. 2013. Vol. 113. P. 27–53. DOI: 10.1007/s10659-012-9409-y

44. *Dasgupta S.*, *Sengupta D.* A higher-order triangular plate bending element revisited. International Journal for Numerical Methods in Engineering. 1990. Vol. 30. P. 419–430. DOI: 10.1002/NME.1620300303

45. Abaqus User Subroutines Reference Guide. Dassault Systèmes, 2016. 683 p.

46. *Barenblatt G.I.* The Mathematical Theory of Equilibrium Cracks in Brittle Fracture. Advances in Applied Mechanics. 1962. Vol. 7. P. 55–129. DOI: 10.1016/S0065-2156(08)70121-2

Authors' Details:

Kirill Shelkov (corr.), Assistant Lecturer and PhD student at Moscow Aviation Institute (National Research University); e-mail: shelkov_k@mail.ru; ORCID: 0009-0003-4618-0633

Yury Solyaev, Doctor of Physical and Mathematical Sciences, Leading Researcher at the Institute of Applied Mechanics of the Russian Academy of Sciences; e-mail: yurysolyaev@ya.ru; ORCID: 0000-0001-8258-2726